JOURNAL OF MATERIALS SCIENCE 23 (1988) 371–379

Anelastic behaviour of materials under multiaxial strains

Part 2 *Poisson's ratio, coupling of strains and anelastic relaxation in Zircaloy-4*

R. E. BOLMARO
Instituto de Fisica Rosario (CONICET-UNR), Facultad de Ciencias Exactas e Ingenieria, Departamento de Fisica, Universidad Nacional de Rosario, Av. Pellegrini 250, (2000) Rosario, Argentina

F. POVOLO*
International Centre for Theoretical Physics, Trieste, Italy

Data on Poisson's ratio as a function of temperature, obtained in rods and tubes of Zircaloy-4 through dynamical measurements in longitudinal excitations, are presented. The influence of texture and the contribution of a coupling between longitudinal and transversal vibrations on the observed temperature dependence of this elastic constant, is discussed. Finally, an anelastic effect produced by relaxation of Poisson's ratio, in the temperature region between 400 and 450 K, is also presented. This effect is present only in tubular specimens and it is discussed in terms of a theory of anelastic relaxation under multiaxial strains.

1. Introduction

The elastic constants of zirconium-rich alloys, used in nuclear applications, have been found to be strongly dependent on texture and to vary comparatively less with alloy content [1–3]. This substantiates the calculation of the elastic constants of zirconium alloys by means of zirconium single crystal data. Generally, a space average of the monocrystal compliance coefficients is used, weighted by the crystallographic pole density and a good agreement with experimental measured values for Young's and shear moduli was encountered [2, 3]. A reasonable agreement is also found when the measured values are compared with those predicted by Voigt and Reuss averages. In fact, it can be stated, in general, that the predicted and measured values for these moduli do not differ by more than 25% [1–6]. Furthermore, a similar situation is found for their temperature dependence where, in addition, the predicted and measured behaviour are substantially the same. This is not the case for Poisson's ratio, however, where the predicted values differ substantially from the experimental data, and it was found for some alloys that the predicted temperature dependence of this elastic constant was opposite to the experimental one [2].

The most recent review on all the elastic constants for zirconium-rich alloys has been presented by Northwood *et al.* [2], even if systematic errors were introduced on calculating Poisson's ratio [7]. The last review, as far as we know, on elastic constants for different metals and alloys, has been presented by Köster and Franz [8] where it can be seen that the situation is quite similar to that encountered in zirconium alloys; that is, the agreement between predicted and measured values is reasonable for Young's and shear moduli, but very poor for Poisson's ratio. This was also pointed out in a recent publication [9], where a general formalism has been presented, to be used to calculate the average elastic constants for a random polycrystal in terms of the elastic constants for the single crystal.

Povolo and Bolmaro [7, 10] have analysed the different values reported in the literature for Poisson's ratio of metals and alloys, showing that this elastic constant is more strongly influenced by anisotropy than Young's and shear moduli. In fact, even negative values were estimated for single crystals. Clearly, in this condition the usual method of obtaining Poisson's ratio for polycrystals, from the measured Young's and shear moduli, through the very well known relationship

$$\nu = (E/2G) - 1 \qquad (1)$$

valid for isotropic solids, might lead to serious errors if preferred orientations are present. E and G are Young's and shear moduli, respectively and ν is Poisson's ratio. It might be possible, also, that ν is more sensitive to impurities, that is, to alloying, particularly for certain orientations.

From the experimental point of view, there are only limited data in the literature on direct measurements of Poisson's ratio. In addition, these data have been

* *Permanent address:* Comision Nacional de Energia Atomica, Departamento de Materiales, Av. Libertador 8250, (1429), Buenos Aires, Argentina, and Facultad de Ciencias Exactas y Naturales, Departamento de Fisica, Universidad de Buenos Aires, Pabellon 1, Ciudad Universitaria, (1428) Buenos Aires, Argentina.

0022–2461/88 $03.00 + .12

obtained by means of a conventional mechanical test, where it is difficult to establish if the specimen has been really deformed in the elastic regime.

It is the purpose of this paper to present data on Poisson's ratio as a function of temperature, for tubes and rods of Zircaloy-4. The measurements were performed by using a resonant method in longitudinal excitation and the results are discussed in terms of theories of elastic vibrations and of anelasticity under multiaxial strains. This last theory has been presented in detail elsewhere [11].

2. Experimental procedure

The longitudinal resonant frequencies were measured by using the "free–free" or floating beam resonant method, described by Spinner and Tefft [12] and Sorrentino [13]. In particular, the electrostatic drive and detection method with a polarizing voltage (condenser microphone arrangement) was used [14–16]. The apparatus was constructed in the laboratory and the supporting device was made of Zircaloy-4 to avoid the influence of dilatations on the interelectrode capacity. The basic electronic instrumentation is shown as a block diagram in Fig. 1 and the details are described elsewhere [17, 18].

The equipment utilizes the capacitive coupling between the specimen and fixed electrodes positioned close to vibration antinodes. Displacement sensitivities of 1 to 2 μm have been obtained at the strain amplitudes of the order of 10^{-8} used for the measurements. Specimens of Zircaloy-4 in the form of cylindrical rods approximately 150 mm long and 12 mm diameter and tubes, normally used as fuel sheating, approximately 150 mm long and 12 mm outer diameter, were used. The densities, ϱ, of all the specimens, determined with a picnometer at 299 K, were $\varrho = 6.680 \pm 0.003\,\mathrm{g\,cm^{-3}}$ for fuel sheatings, and $\varrho = 6.587 \pm 0.003\,\mathrm{g\,cm^{-3}}$ for rods. The frequency can be determined with a relative error of the order of 5×10^{-4}, introduced mainly by the suspension point. The relative errors in the determination of the rest of the magnitudes involved are: 1×10^{-6} on the lengths, 2×10^{-5} on the diameters and 5×10^{-4} on the densities. The temperature was controlled, between room temperature and 723 K, with a proportional controller which gave an accuracy of ± 2 K. This indetermination in the temperature implies a relative error of the order of

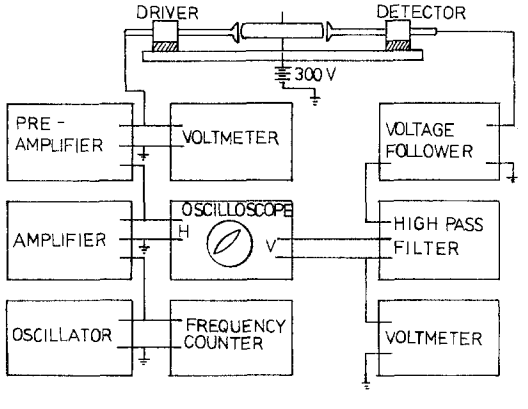

Figure 1 Block diagram of the basic electronic instrumentation.

TABLE I Dimensions of the tubes and rods used

Specimen	r_i(mm)	r_o(mm)	L(mm)
P-1-V			149.941
P-2-V			150.017
P-3-V	5.39	5.95	149.958
P-4-V			149.982
P-5-V			149.745
P-1-M			149.883
		6.185	
P-2-M			149.959

2×10^{-5} on the frequencies, which is smaller than the error introduced by the suspension point.

The complete solution of the equation of motion for the propagation of free harmonic waves along a hollow cylinder of finite extent, leads to an implicit transcendental function of the type [19]

$$\phi = \phi(E, \nu, \varrho, L, f_j, r_i, r_o) = 0 \qquad (2)$$

where L is the length of the cylinder, r_i and r_o are the inner and outer diameters, respectively, and f_j is the resonant frequency where $j = 1, 2, 3...$ gives the order of the harmonics for a specimen suspended in the centre. Equation 2 cannot be solved algebraically for f_j, in terms of the properties of the material and the dimensions of the specimen, and must be solved numerically. The case of cylindrical rod is also represented by Equation 2 with $r_i = 0$. The dimensions of the specimen used are given in Table I. In most cases, the resonant frequencies are given accurately enough by the expression

$$f_j = \frac{j}{2L}(E/\varrho)^{1/2}\left[1 - \frac{j^2\pi^2\nu^2}{4L^2}(r_i + r_o)^2\right] \qquad (3)$$

or, even by the simplest solution

$$f_j = \frac{j}{2L}(E/\varrho)^{1/2} \qquad (4)$$

In principle, Poisson's ratio can be obtained from Equation 3 by measuring the resonant frequencies at two different harmonics, j and j^*, and solving for ν, that is

$$\nu = [(j^* f_j - j f_{j^*})/(j^{*3} f_j - j^3 f_{j^*})]^{1/2} \times [2L/\pi(r_i^2 + r_o^2)^{1/2}] \qquad (5)$$

on assuming that E is independent of frequency.

The simplest solutions to the wave equation, given by Equations 3 and 4, give good values for E, as calculated from the measured f_j, the properties of the material and the dimensions of the specimen. This was found to be the case for rods and, to a lesser extent for tubes, where the deviation between the measured frequencies and those predicted by Equation 3 or 4 increases with the order of the harmonics [19].

Some comments should be made next about the influence of the thermal expansion on the results. In fact, if Young's modulus is calculated from the measured resonant frequencies by using the first-order approximation given by Equation 4, then, the influence of the thermal expansion is represented by

$$E_{T_2} = 4L_{T_1}^2[1 + \alpha(T_2 - T_1)]^2 \times f_{jT_2}^2 \varrho_{T_1}/[1 + 3\alpha(T_2 - T_1)] \qquad (6)$$

TABLE II Relative error of Poisson's ratio, ε_ν, obtained by propagation of the error in the measurements of the frequencies into Equation 4

ε_ν(%)	j	j^*
17	1	3
9	3	5
5	5	7
3	7	9
7	9	11

where T_1 is the room temperature, T_2 is the temperature at which the resonant frequency is measured and α is the linear thermal expansion coefficient. The correction to Young's modulus, implied by Equation 6, is less than 2.5×10^{-3}, in the temperature region considered in the paper. The use of the second-order approximation, that is, if the influence of thermal expansion is introduced into Equation 3, leads to a smaller correction. Moreover, corrections due to thermal expansion are not necessary in the evaluation of Poisson's ratio, to a first approximation, because the $(1 + \alpha T)$ dependence of L and r compensates each other.

Finally, even if the resonant frequencies are determined with a relative error of the order of 5×10^{-4}, the error propagated on Poisson's ratio is, in several cases, greater than the repetitiveness of the measurements. In fact, on considering Equation 5, for example, and using classical calculations for the propagation of errors, the results given in Table II are obtained for the relative error, ε_ν, on Poisson's ratio. Such a large dispersion on the results, however, was not obtained experimentally because the statistical dispersion, point to point, is eliminated by the special mathematical procedure used. In fact, E and ν were calculated from the measured frequencies by solving numerically Equation 2 and using an iterative procedure [19]. A maximum relative error of the order of 5% is expected, in the most unfavourable situation.

3. Results

3.1. Tubes

Fig. 2 shows the values obtained for Young's modulus as a function of temperature and at three different harmonics, in tube P-1-V. Harmonics 5 and 9 are not indicated to avoid superposition. These values have been calculated by solving numerically

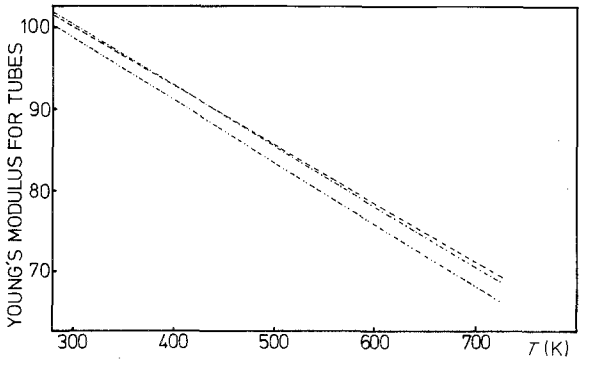

Figure 2 Young's modulus as a function of temperature for j = (– – –)1, (– · –)3 and (– · – · –)7, calculated by using Equation 2 and the measured frequencies. Specimen P-1-V.

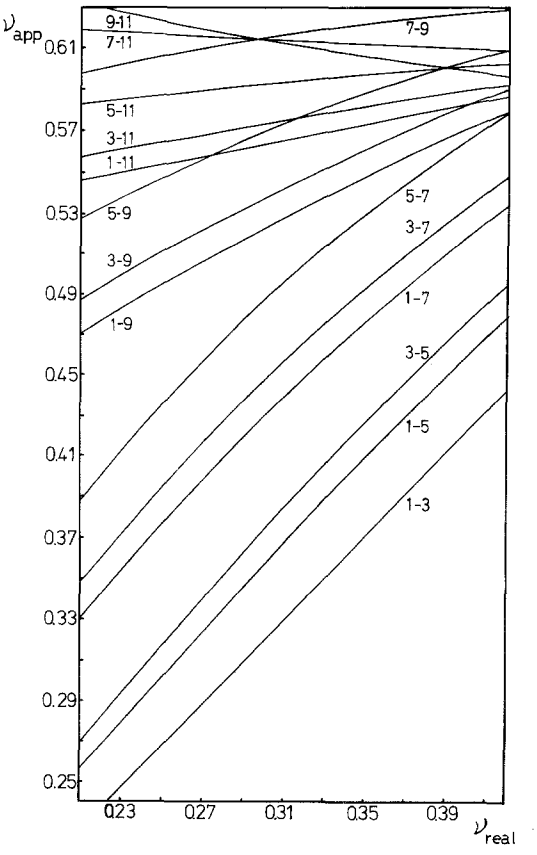

Figure 3 Comparison between the values for Poisson's ratio obtained by using Equation 5, ν_{app}, with those given by a numerical solution of Equation 2, ν_{real}, for tube P-1-V. The pair of harmonics used to calculate each curve are indicated.

Equation 2 and using the measured frequencies. A linear regression analysis of all the data points leads to the following expressions for the temperature dependence of Young's modulus, measured at the different frequencies:

$$\begin{aligned} E_1 &= 101.485 - 0.07085\,(T - 273\,\mathrm{K}) \\ E_3 &= 101.692 - 0.07309\,(T - 273\,\mathrm{K}) \\ E_5 &= 101.554 - 0.07586\,(T - 273\,\mathrm{K}) \\ E_7 &= 101.077 - 0.07724\,(T - 273\,\mathrm{K}) \\ E_9 &= 101.083 - 0.07488\,(T - 273\,\mathrm{K}) \end{aligned} \quad (7)$$

Equations 7 and Fig. 2 show that the value obtained for Young's modulus does not depend strongly on the harmonics selected and almost the same temperature dependence is obtained for each resonant frequency. Moreover, similar results would be obtained by using the approximate Equations 3 and 4. The situation is completely different for Poisson's ratio, however, where the complete equation, i.e. Equation 2, must be used. In fact, Fig. 3 shows a comparison between the values obtained for Poisson's ratio, ν_{app}, on using the approximate Equation 5 with those obtained by solving numerically Equation 2, which are indicated by ν_{real}. The pair of harmonics used for each curve are also indicated in the same figure. ν_{real} gives the values of Poisson's ratio without the influence of shape effects and ν_{app} was obtained by fitting the E against T curves, at each harmonic, by linear regression analysis, taking pairs of curves and solving the square root of Equation 5 by approximating it with a second-

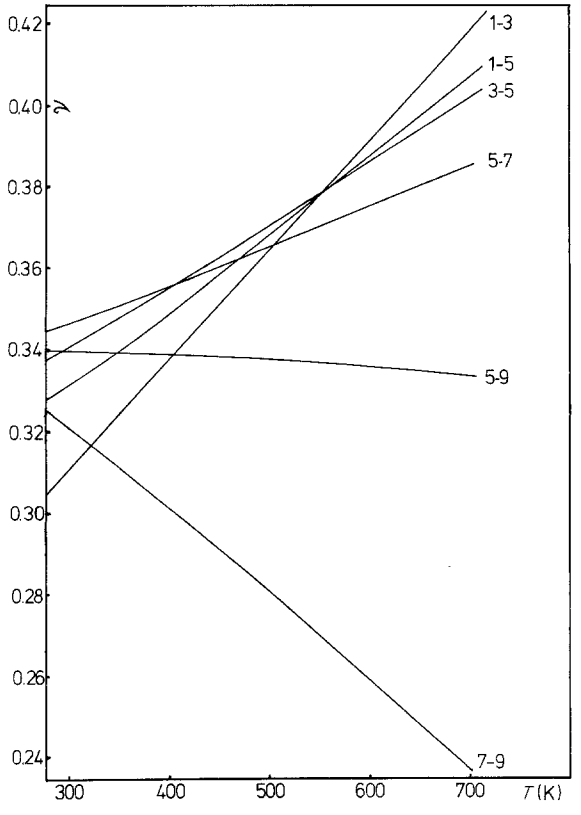

Figure 4 Poisson's ratio for tube P-1-V as a function of temperature and frequency. The pair of harmonics used are indicated on each curve.

degree polynomial. This procedure reduces the aleatory error in each point. Fig. 4 shows a plot of ν_{real} against temperature, where the subscript has been omitted for simplicity. Only results corresponding to adjacent frequencies will be considered in what follows to avoid any possible influence of a frequency dependence of Young's modulus on the results.

A more careful analysis of the experimental data shows a discontinuity in the general temperature dependence of the resonant frequencies, in the temperature region between about 400 and 450 K. This is illustrated in Fig. 5, where the temperature dependence of the square of the normalized frequencies, for harmonics 1 and 7, is shown. f_{j0} indicates the corresponding frequency obtained at room temperature. A linear regression in the two sections, indicated by the straight lines, leads to correlation coefficients nearer to one than for the case where only one straight line is considered at all the temperatures and for each harmonic. This discontinuity in the resonant frequencies is reflected and magnified in the temperature dependence of Poisson's ratio, as calculated with the procedure described previously. This is illustrated by Fig. 6, where ν has been calculated for adjacent harmonics on taking into account the discontinuities observed on the temperature dependence of the different resonant frequencies. The results shown are representative of the data obtained in all the tubular specimens investigated.

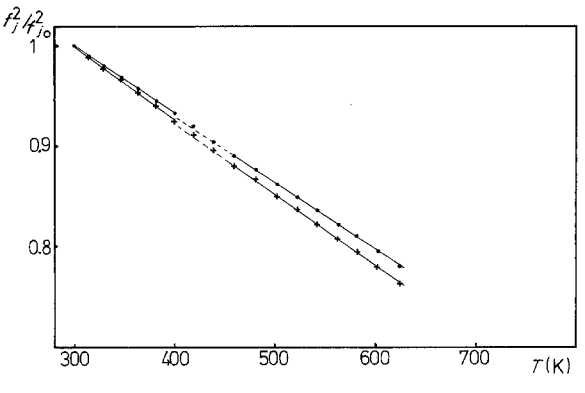

Figure 5 Discontinuity in the temperature dependence of the resonant frequencies for tube P-1-V. (●) $j = 1$; (+) $j = 7$.

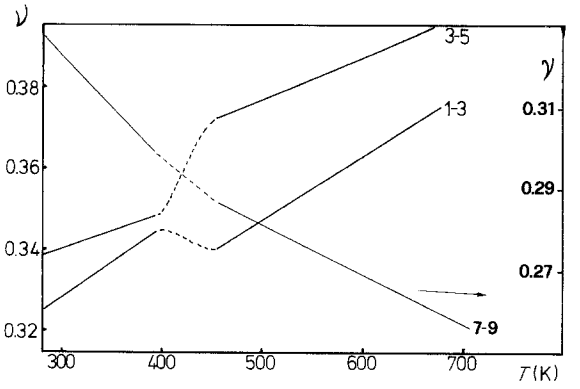

Figure 6 Temperature dependence of Poisson's ratio for tube P-1-V, on considering the discontinuities in the measured temperature dependence of the resonant frequencies. The pair of harmonics used for the calculation of ν are indicated on each curve.

3.2. Rods

Fig. 7 shows typical results obtained for Young's modulus in cylindrical specimens. The curve shown is the average over all the harmonics, because only minor differences were obtained at the various resonant frequencies. A linear regression through all the data points leads to the following expression for the straight line shown in Fig. 7

$$E = 99.366 - 0.06417\,(T - 273\,\mathrm{K}) \qquad (8)$$

The corrected values for Poisson's ratio, obtained for each pair of harmonics, are shown in Fig. 8, where it can be seen that Poisson's ratio does not fall more rapidly with temperature on increasing the frequency, as observed in tubes, and the measured curves have practically the same slope for the different overtones.

3.3. Drilled cylindrical rods

In order to study the transition from the cylindrical rod to the tube, the rod was drilled longitudinally,

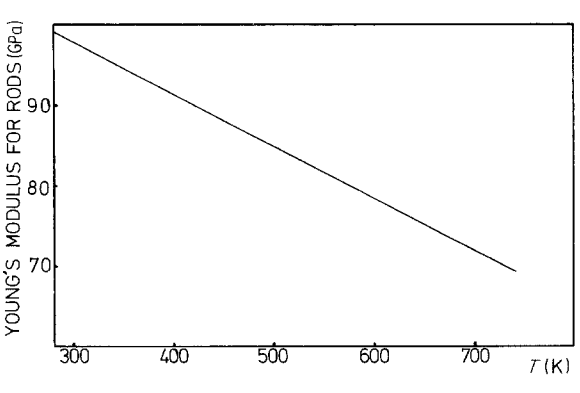

Figure 7 Temperature dependence of Young's modulus for cylindrical rods, obtained at all frequencies.

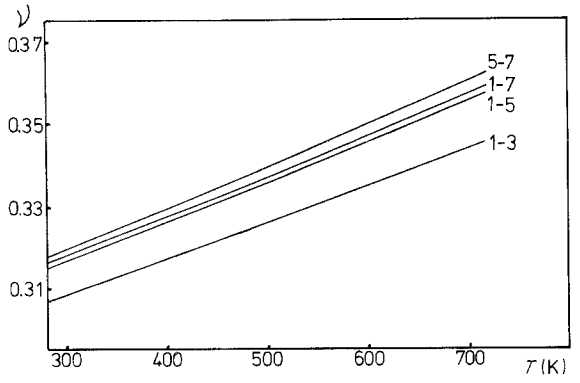

Figure 8 Poisson's ratio as a function of temperature for cylindrical rods and different combinations of harmonics.

to form tubes with different dimensions. Seven successively increasing diameters were drilled and the resonant frequencies were measured as a function of temperature. It was observed that the frequencies for the higher overtones decreased more rapidly with temperature as the inner diameter increased. The temperature and frequency dependence of Poisson's ratio, at two different inner diameters, are shown in Figs 9 and 10. These figures show that the dispersion in the values of Poisson's ratio, for the different harmonics, increases as the inner diameter increases, and ν decreases at high temperatures and at the higher overtones, on going from the rod to the tube, i.e. when the inner diameter increases (compare Figs 9 and 10 with Figs 4 and 8).

4. Discussion

There are two effects contributing to the observed change in the measured values for Poisson's ratio, with temperature and frequency, shown in Fig. 6: an anelastic relaxation of Poisson's ratio and a coupling between the different overtones produced mainly by the anisotropy, that is, by the texture of the specimen. Povolo and Bolmaro [11] have recently developed a theory of anelasticity under multiaxial strains. According to this theory, if the angle θ formed between the direction of the applied sinusoidal stress and the $\langle c \rangle$-axis of the hexagonal crystal is $\pi/2$, i.e. if the excitation is perpendicular to this axis, the strains produced are given by

$$\varepsilon_3' = \left[s_{11} + \left(s_{11} - \frac{\delta}{2} \right) \omega^2 \tau^2 - i\omega\tau \frac{\delta}{2} \right] \Big/ [1 + \omega^2 \tau^2] \tag{9}$$

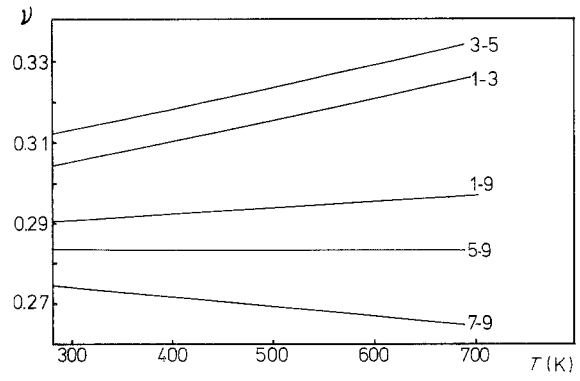

Figure 9 Poisson's ratio for a drilled rod with an internal diameter of 3.5 mm.

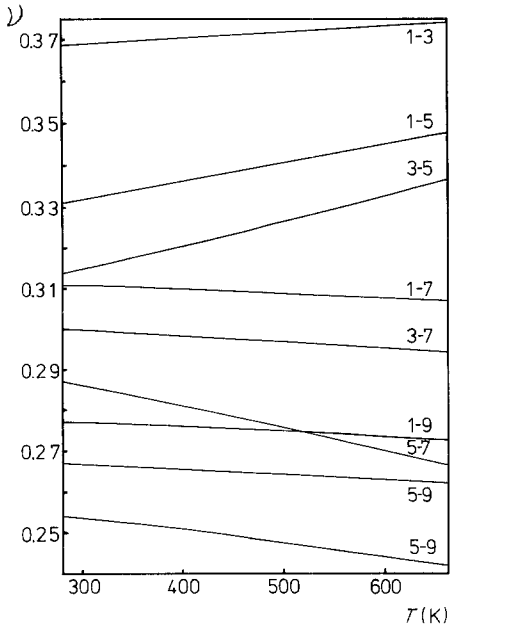

Figure 10 Poisson's ratio for a drilled rod with an internal diameter of 4.5 mm.

$$\varepsilon_1' = \Big[(s_{12} \cos^2\psi + s_{13} \sin^2\psi) + \left(s_{12} \cos^2\psi + s_{13} \sin^2\psi + \frac{\delta}{2} \cos^2\psi \right) \omega^2 \tau^2 + i\omega\tau \frac{\delta}{2} \cos^2\psi \Big] \Big/ [1 + \omega^2 \tau^2] \tag{10}$$

where ε_3' is the strain in the direction of the applied stress and ε_1' in a perpendicular direction. δ represents the intensity and τ the time, at constant stress, for the relaxation of $(s_{11} - s_{12})$, ω is the angular frequency of the applied stress and s_{ij} are the compliances of the hexagonal crystal. ψ indicates the direction in the plane whose normal is in the direction of the applied stress [7, 10, 11]. θ and ψ are two of the Eulerian angles that define the orientation of the excitation with respect to the coordinate system referred to the hexagonal cell. For $\psi = 0$ the complex Poisson's ratio is given by

$$\nu_0' = -\varepsilon_1'/\varepsilon_3' = \nu_0^{(1)} - i\nu_0^{(2)} = -\left[s_{11}s_{12} + \left(s_{11} - \frac{\delta}{2} \right) \times \left(s_{12} + \frac{\delta}{2} \right) \omega^2 \tau^2 \right] \Big/ \left[s_{11}^2 + \left(s_{11} - \frac{\delta}{2} \right)^2 \omega^2 \tau^2 \right] - i\omega\tau\delta \Big/ \left[s_{11}^2 + \left(s_{11} - \frac{\delta}{2} \right)^2 \omega^2 \tau^2 \right] \tag{11}$$

It is easy to show from Equation 11 that

$$\begin{aligned} \omega\tau \to 0 \quad & \nu_0^{(1)} = -s_{12}/s_{11} \\ \Rightarrow & \\ \omega\tau \to \infty \quad & \nu_0^{(1)} = -\left(s_{12} + \frac{\delta}{2} \right) \Big/ \left(s_{11} - \frac{\delta}{2} \right) \end{aligned} \tag{12}$$

In addition, the curve of $\nu_0^{(1)}$ against $\omega\tau$ has an inflection point at

$$\omega\tau = \frac{1}{3^{1/2}} \left[s_{11} \Big/ \left(s_{11} - \frac{\delta}{2} \right) \right] \tag{13}$$

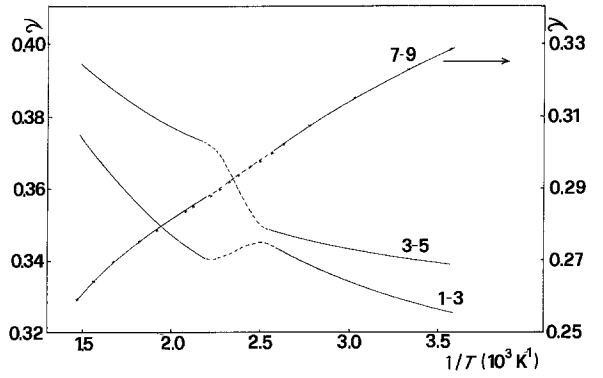

Figure 11 Poisson's ratio as a function of the reciprocal of the absolute temperature, as obtained from the data of Fig. 6.

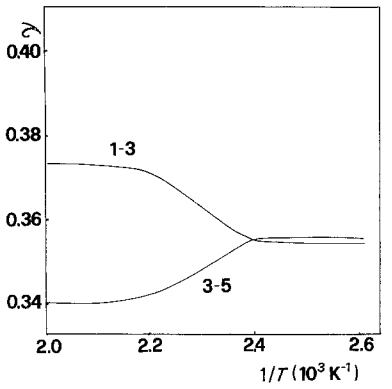

Figure 12 Anelastic relaxation of Poisson's ratio, as obtained by subtracting out the background from the curves of Fig. 11.

For $\psi = \pi/2$ the complex Poisson's ratio is given by

$$\nu_{\pi/2} = -\varepsilon_1'/\varepsilon_3' = \nu_{\pi/2}^{(1)} - i\nu_{\pi/2}^{(2)}$$
$$= -s_{13}\left[s_{11} + \left(s_{11} - \frac{\delta}{2}\right)\omega^2\tau^2\right] \Big/ \left[s_{11}^2 + \left(s_{11} - \frac{\delta}{2}\right)^2\omega^2\tau^2\right]$$
$$- i\omega\tau\delta/2\left[s_{11}^2 + \left(s_{11} - \frac{\delta}{2}\right)^2\omega^2\tau^2\right] \qquad (14)$$

Equation 14 leads to

$$\begin{array}{lll} \omega\tau \to 0 & \nu_{\pi/2}^{(1)} = -s_{13}/s_{11} \\ \Rightarrow & \\ \omega\tau \to \infty & \nu_{\pi/2}^{(1)} = -s_{13}\Big/\left(s_{11} - \dfrac{\delta}{2}\right) \end{array} \qquad (15)$$

The inflection point is also given in this case by Equation 13. The real part of ν, i.e. $\nu^{(1)}$, leads to a curve similar to the one found for J_1 in the dynamic response of the standard anelastic solid [11, 20]. $\nu^{(2)}$ leads to a Debye peak similar to the response function J_2. In addition, $\nu_0^{(1)}$ decreases and $\nu_{\pi/2}^{(1)}$ increases as $\omega\tau$ increases. On taking into account the values for the elastic constants of zirconium single crystals, reported by Fisher and Renken [21], at 450 K, it is easy to show that

$$\nu_0^{(1)}(\omega\tau \to 0) = -s_{12}/s_{11} = 0.453 \qquad (16)$$
$$\nu_{\pi/2}^{(1)}(\omega\tau \to 0) = -s_{13}/s_{11} = 0.194 \qquad (17)$$

Moreover, if the temperature dependence of τ is taken, as is usually done [20], as

$$\tau = \tau_0 \exp(\Delta H/kT) \qquad (18)$$

where τ_0 is the pre-exponential factor and ΔH the activation enthalpy, then

$$\ln(\omega\tau) = \ln(\omega\tau_0) + (\Delta H/kT) \qquad (19)$$

showing that $\ln(\omega\tau)$ changes linearly with T^{-1}, which means that as $\omega\tau$ increases, T^{-1} increases (T decreases). the data of Fig. 6 are plotted as a function of T^{-1} in Fig. 11, where the discontinuities in the temperature dependence of Poisson's ratio are evident, in the temperature region between about 400 and 450 K, for the values obtained for harmonics 1 to 3 and 3 to 5. This is not so clear for the combination of harmonics 7 to 9. Fig. 12 shows the curve obtained by extrapolating the smooth decrease at high temperatures, by considering it as a background up to where the new background at low temperatures is present, after the sudden change. This procedure shows that ν decreases from about 0.374 to 0.354 for harmonics 3 to 5. For harmonics 1 to 3, however, ν increases from about 0.34 to 0.356. It should be pointed out that the theoretical values, given by Equations 16 and 17, correspond to single crystals, which is not the case because polycrystalline specimens were used to obtain the data presented and the texture of the material should be considered.

Curve 1–3 of Fig. 12 shows the typical behaviour expected for $\nu_{\pi/2}^{(1)}$ and curve 3–5 the general trend expected for $\nu_0^{(1)}$. Moreover, on taking into account Equations 12 and 15 it is possible to calculate δ/s_{11} from the measured asymptotic values, for each curve. The following values are obtained

$$\delta/s_{11} = 9 \times 10^{-2} \quad \text{for curve 1–3} \qquad (20)$$
$$\delta/s_{11} = 6 \times 10^{-2} \quad \text{for curve 3–5} \qquad (21)$$

showing that similar values are obtained for δ from both curves. In addition, the order of magnitude of the relaxation measured seems reasonable when compared with data reported in the literature for measurements obtained from the relaxation behaviour of Young's and shear moduli [20]. This would confirm the interpretation given in the paper of the abrupt change observed in the temperature dependence of Poisson's ratio in the temperature region between about 400 and 450 K, i.e. as being produced by anelastic relaxation. It is interesting to notice how the small perturbation present in the resonant frequencies, as indicated in Fig. 5, is magnified when Poisson's ratio is considered. This would indicate that the defect responsible for the anelastic effects produces a distortion which is maximum in a direction perpendicular to the applied stress. It is clear that more information is needed in order to obtain additional characteristics of the defect involved in the relaxation process.

It should be pointed out that the calculations performed are only approximate because, as pointed out before, textured polycrystals were used for the measurements. In fact, Equations 12 and 13 assume that the specimen is a single crystal and that the sinusoidal stress is applied along specific directions. This is not the case for the tubes and rods used for the measurements, which are not only polycrystalline but,

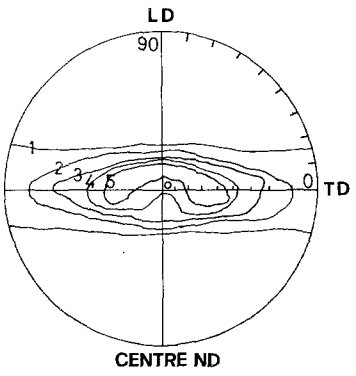

Figure 13 (0 0 0 2) pole figure for Zircaloy-4 tubes.

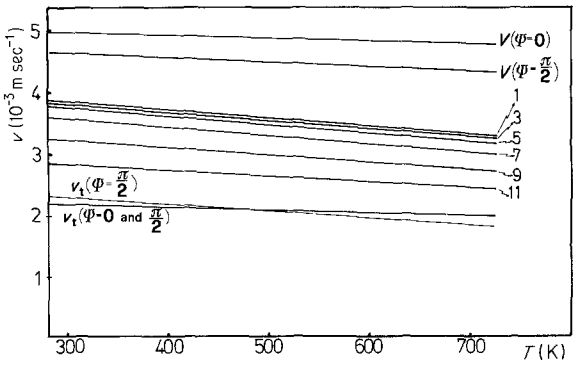

Figure 14 Longitudinal, v_l, and transversal velocities, v_t, as a function of temperature, for the propagation of elastic waves in zirconium single crystals. Curves 1 to 11 indicate the average velocities, for longitudinal excitations, calculated with Equation 26.

in addition, preferred orientations are present. Fig. 13 gives the (0 0 0 2) pole figure for the tubes, as determined by the Schulz technique. It is seen that the $\langle c \rangle$-axis of the hexagonal crystals that form the polycrystal are oriented near the normal direction, between the longitudinal and transversal directions of the tube, as extremes. On remembering that the tubes are excited in the longitudinal direction it is seen that the conditions implied by Equations 9 to 15 are nearly fulfilled. It should be taken into account, however, that the observed temperature dependence of Poisson's ratio, shown in Figs 4, 6 and 11 is due to several effects. In fact, there is an anelastic contribution due to the relaxation of v, typified by the extreme orientations considered and another contribution due to coupling between longitudinal and transverse vibrations, produced by the particular texture present in the specimens. In fact, on solving Equation 2 it was assumed that the material is isotropic, which is certainly not the case.

In order to get an idea of the influence of anisotropy on the results, it is possible to solve the wave equation for hexagonal crystals, by using elasticity theory of crystal vibrations. In fact, the velocities for the propagation of elastic waves in crystals can be calculated with the classical equation [22]

$$(\varrho\omega^2\delta_{im} - c_{iklm}k_k k_l)u_m = 0 \qquad (22)$$

where u_m are the components of the displacement vector, c_{iklm} are the elastic constants and k_k are the components of the wave vector. The three normal vibration modes can be calculated by solving the secular equation

$$|c_{iklm}k_k k_l - \varrho\omega^2\delta_{im}| = 0 \qquad (23)$$

with $\boldsymbol{k} = (k_x, k_y, k_z)$ forming an angle θ with the $\langle c \rangle$-axis of the crystal. θ is the angle between the z-axis (which is along the sixth-order axis of the crystal) and the wave vector $\boldsymbol{k}$. Then, $k_x = 0$, $k_y = k \sin\theta$ and $k_z = k \cos\theta$. If $\theta = \pi/2$ then $k = (0, k, 0)$ and the three normal modes are

$$\begin{aligned} \omega_t &= \omega_1 = k[(c_{11} - c_{12})/2\varrho]^{1/2} & u_1 &= (1,0,0) \\ \omega_l &= \omega_2 = k(c_{11}/\varrho)^{1/2} & u_2 &= (0,1,0) \\ \omega_t &= \omega_3 = k(c_{44}/\varrho)^{1/2} & u_3 &= (0,0,1) \end{aligned} \qquad (24)$$

where l and t indicate longitudinal and transversal vibrations, respectively. If $\theta = 0$ then $\boldsymbol{k} = (0, 0, k)$ and the three normal modes are

$$\begin{aligned} \omega_t &= \omega_1 = k(c_{44}/\varrho)^{1/2} & u_1 &= (1,0,0) \\ \omega_t &= \omega_2 = k(c_{44}/\varrho)^{1/2} & u_2 &= (0,1,0) \\ \omega_l &= \omega_3 = k(c_{33}/\varrho)^{1/2} & u_3 &= (0,0,1) \end{aligned} \qquad (25)$$

The normal vibration modes are perpendicular and the velocities of propagation can be calculated, as a function of temperature, by using the elastic constants for zirconium single crystals reported by Fisher and Renken [21]. These velocities are shown in Fig. 14, as calculated with Equations 24 and 25 between room temperature and 723 K.

On forcing longitudinal vibrations in the tube the wavelength is determined by the length of the specimen and the frequencies are imposed by the driver. The wave vector is along the longitudinal axis of the specimen and the dispersion relationship $\omega(k)$ is given by

$$\omega(k)/k = 2f_j L(1 + \alpha T)/j \qquad (26)$$

The average velocities of the longitudinal waves, calculated with Equation 26 for the different harmonics, by using the measured frequencies, are also shown in Fig. 14. These velocities are average values not only over the longitudinal anisotropy but over the transversal anisotropy too, due to coupling with transversal vibrations. The average velocities are located in between those of the transverse and longitudinal modes of the single crystal. The frequency of the higher overtones falls more rapidly with temperature than in solid bars, due to the coupling with the transversal vibrations, particularly at high temperatures. In fact, as shown elsewhere [7], Poisson's ratio increases strongly with temperature for a contraction in the direction of the $\langle c \rangle$-axis and decreases more slowly for a contraction in a perpendicular direction. These two particular orientations are present in the fuel sheating and the coupling occurs, at low frequencies, with a transversal strain perpendicular to the $\langle c \rangle$-axis of the crystals forming the polycrystals. At high frequencies, on the contrary, the coupling occurs with a transversal strain perpendicular to the $\langle c \rangle$-axis, particularly at high temperatures. The coupling effect is not obvious at

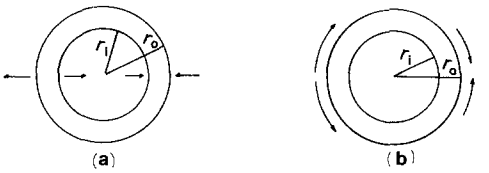

Figure 15 Coupling between longitudinal and transversal vibrations in tubes. (a) low frequencies; (b) high frequencies.

low temperatures because of the small differences between both Poisson's ratios. These two extreme coupling situations are illustrated schematically in Fig. 15. Furthermore, the coupling effects influence the observed temperature dependence of ν and the asymptotic values measured experimentally, which differ from the theoretical values given by Equations 16 and 17.

A different situation is encountered for rods, where a poor coupling with transversal vibrations is observed and only the transversal mode along the $\langle c \rangle$-axis is activated. In fact, Fig. 16 gives the usual texture obtained in rods, as measured by neutron diffraction by Mac Ewen and Tomé [23] for Zircaloy-4. It shows a classical random distribution of the $\langle c \rangle$-axis over a plane perpendicular to the longitudinal axis of the specimen. From the measured temperature dependence of the different resonant frequencies and of Poisson's ratio, it can be concluded that ν is only sensitive to transversal strains in the direction of the $\langle c \rangle$-axis.

Finally, Figs 17 and 18 show the texture measured in a drilled rod, at two different drilled holes, with diameters similar to those used for the data shown in Figs 9 and 10. The texture was determined by cutting out a ring, flattening it and determining the preferred orientation in the inner surface. It can be seen that the texture approaches that observed in fuel sheatings, as the inner diameter increases. In fact, the (0 0 0 2) poles approach the radial direction, starting from a random distribution between the radial and tangential directions. As shown by Figs 9 and 10, changes, as expected, from the behaviour observed in rods to the trend observed in tubes.

5. Conclusions

An anelastic effect produced by relaxation of Poisson's ratio has been observed in Zircaloy-4 tubes, in the temperature region between about 400 and 450 K. This effect is strongly anisotropic and the temperature dependence of Poisson's ratio is influenced by the texture of the specimen, because of coupling effects between longitudinal and transversal vibrations. No anelastic phenomena in the temperature dependence of Poisson's ratio have been observed in Zircaloy-4 rods, because of the particular texture involved.

It has been shown that the experimental values obtained for Poisson's ratio, through dynamical experiments, must be analysed in detail because of the influence of various contributions to the measured temperature dependence.

Finally, no specific mechanism is given for the defects responsible for the observed anelasticity, which is magnified in Poisson's ratio with respect to Young's modulus, because more experimental data are needed particularly in single-crystal specimens with different orientations.

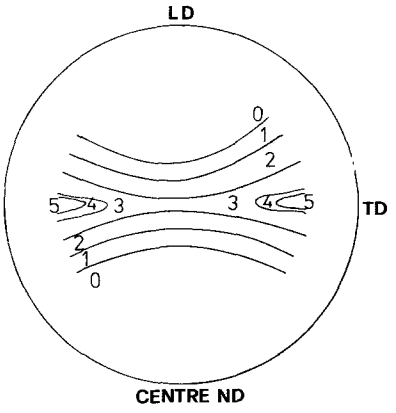

Figure 17 (0 0 0 2) pole figure for a drilled rod with r_i = 3.7 mm.

Acknowledgements

The authors would like to thank Dr. R. Migoni for his helpful comments. One of the authors (F. P.) thanks Professor Abdus Salam, the International Atomic Energy Agency and UNESCO for hospitality at the International Centre for Theoretical Physics, Trieste, where part of the manuscript was completed. This work was supported in part by the Consejo Nacional de Investigaciones Cientificas y Tecnicas (CONICET), the Comision de Investigaciones Cientificas de la Provincia de Buenos Aires (CIC) and the "Proyecto Multinacional de Tecnologia de Materiales" OAS-CNEA.

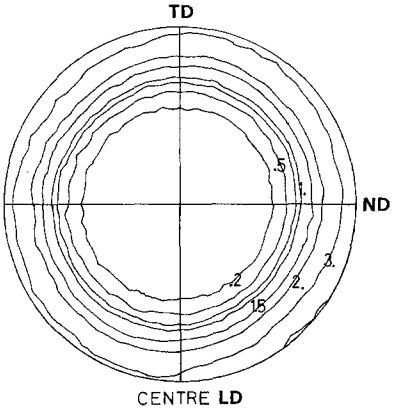

Figure 16 (0 0 0 2) pole figure for Zircaloy-4 cylindrical rods.

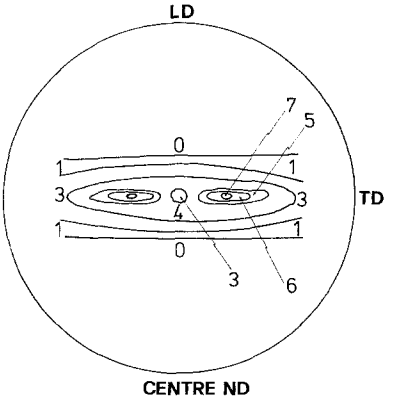

Figure 18 (0 0 0 2) pole figure for a drilled rod with r_i = 5 mm.

References

1. H. E. ROSINGER, I. G. RITCHIE and A. J. SHILLINGLAW, Atomic Energy of Canada Limited, Report AECL-5231 (September 1975).
2. D. O. NORTHWOOD, I. M. LONDON and L. E. BAHEN, *J. Nucl. Mater.* **55** (1975) 299.
3. H. S. ROSENBAUM and J. LEWIS, *ibid.* **67** (1977) 273.
4. P. E. ARMSTRONG and H. L. BROWN, *Trans. AIME* **230** (1964) 962.
5. L. R. BURNELL, J. L. BATES and G. B. MELLINGER, *J. Nucl. Mater.* **116** (1983) 219.
6. J. A. RAYFIELD, BSc thesis, University of Toronto (1966).
7. F. POVOLO and R. E. BOLMARO, *J. Nucl. Mater.* **118** (1983) 78.
8. W. KÖSTER and H. FRANZ, *Metall. Rev.* **6** (21) (1961) 1.
9. F. POVOLO and R. E. BOLMARO, *Phys. Status Solidi,* in press.
10. *Idem,* "Strength of Metals and Alloys", Vol. 1 edited by H. J. McQueen, J.-P. Bailon, J. I. Dickson, J. J. Jonas and M. G. Akben (Pergamon, Toronto, 1985) p. 287.
11. R. E. BOLMARO and F. POVOLO, *J. Mater. Sci.* **23** (1988) 93.
12. S. SPINNER and W. E. TEFFT, *Proc. ASTM* **61** (1961) 1221.
13. F. SORRENTINO, C. E. N. GRENOBLE, Report CEA-R-3986 (1971).
14. D. BANCROFT and R. C. JACOBS, *Rev. Sci. Instrum.* **9** (1938) 279.
15. R. CABARAT, L. GUILLET and R. LE ROUX, *J. Inst. Metals* **75** (1948-49) 391.
16. R. CABARAT, P. GENCE, L. GUILLET and R. LE ROUX, *ibid.* **80** (1951-52) 151.
17. R. E. BOLMARO, Master Thesis, University of Rosario, Argentina (1981).
18. A. OLIVERO, A. de la TORRE and R. E. BOLMARO, Instituto de Física Rosario (CONI-CET-UNR), Report IFIR-MF 2/82 (1982).
19. F. POVOLO and R. E. BOLMARO, *J. Nucl. Mater.* **116** (1983) 166.
20. A. S. NOWICK and B. S. BERRY, "Anelastic Relaxation in Crystalline Solids" (Academic, New York, 1972).
21. E. S. FISHER and C. J. RENKEN, *Phys. Rev.* **135** (1964) A482.
22. L. D. LANDAU and E. M. LIFSHITZ, "Theory of Elasticity" (Addison-Wesley, Bristol, 1964).
23. S. R. Mac EWEN and C. N. TOMÉ, Proceedings 7th Conference on Zirconium Alloys in Nuclear Industry (Strasbourg, 1985).

Received 24 November 1986
and accepted 29 January 1987